Optimisation of Coanda Surfaces for Transonic Circulation Control

M. Forster⋆†, *M. Biava*⋆⋆ *and R. Steijl*⋆⋆⋆
⋆*PhD. Student. mforster@liv.ac.uk*
⋆⋆*Research Associate. mbiava@liv.ac.uk*
⋆⋆⋆*Lecturer. rsteijl@liv.ac.uk*
CFD Lab, School of Engineering, University of Liverpool, L69 3GH, U.K.
†Corresponding author

Abstract

Gradient based optimisation of a Coanda surface for a transonic, supercritical circulation control aerofoil is presented. Design variable updates are driven by a Sequential Least Squares Quadratic Programming (SLSQP) algorithm, using gradients provided by the solution of the Adjoint equations in discrete formulation. Surface sensitivities of the lift coefficient relative to local variations on the Coanda shape are shown, which indicate that the effects due to under-expansion of the jet have a significant influence on the circulation control efficiency. It is also shown that a 16% improvement in the augmented lift coefficient compared with a simple circular shape can be achieved with minor alterations of an initial quasi-elliptical design. A gain in lift coefficient of $C_l = 0.09$ was achieved relative to this initial shape.

Nomenclature

α	Angle of Attack, degrees
α_{AIL}	Aileron Deflection, degrees
A	Wing Surface Area, m^2
β	Bernstein Coefficient
c	Chord Length, m
C_d	Sectional Drag Coefficient
C_l	Sectional Lift Coefficient
C_m	Sectional Pitching Moment Coefficient
C_μ	Momentum Coefficient, $\frac{\dot{m}_j V_j}{q_\infty A}$
C_p	Pressure Coefficient
ΔC_l	Change in Lift Coefficient due to Blowing
I	Optimisation Objective Function
$\boldsymbol{\lambda}$	Adjoint Vector Variable
M	Freestream Mach Number
$\dot{m}_j$	Jet Mass Flow Rate, kg/s
q_∞	Freestream Dynamic Pressure, Pa
r	Coanda Radius, m
$\boldsymbol{R}$	Residual Vector of the Navier–Stokes Equations
Re	Reynolds Number
θ	Angle from Slot Exit, radians
V_j	Jet Velocity, m/s
$\boldsymbol{W}$	Vector of Flow Variables
$\mathbf{x}$	Vector of Design Variables
y^+	Non-Dimensional Wall Distance

Abbreviations

BFGS	Broyden–Fletcher–Goldfarb–Shanno
CC	Circulation Control
CFD	Computational Fluid Dynamics
EXP	Experiment
HMB	Helicopter Multi-Block CFD Code
IDW	Inverse Distance Weighting
NPR	Nozzle Pressure Ratio
RANS	Reynolds Averaged Navier–Stokes
SLSQP	Sequential Least Squares Quadratic Programming
STOL	Short Take-Off and Landing
UAV	Uninhabited Air Vehicle

Copyright © 2015 by M. Forster, M. Biava and R. Steijl. Published by the EUCASS association with permission.

1. Introduction

Circulation control (CC) is a means of flow control, which typically involves blowing a jet of air over a circular surface at the trailing edge of an aerofoil (Fig. 1). At subsonic speeds, circulation control devices can generate up to three times the lift of conventional mechanical flaps.[1] The potential of circulation control to replace flaps and ailerons has been demonstrated on a low speed UAV.[2] In the transonic flow regime, however, the effectiveness of circulation control is reduced.[3]

We aim to perform an optimisation of the Coanda shape using a supersonic jet and a transonic freestream, with the intention that the design will be suitable for use over the whole flight envelope. From Fig. 2, it is expected that while blowing over the transonic-designed Coanda will not give superior performance in the subsonic regime, the performance may however be sufficient for take-off and landing.

The effect of the shape of the Coanda device appears to be of significant importance to the abilities of the circulation control system for transonic speeds. Parameters such as slot height to radius ratio and rates of curvature influence the detachment phenomenon and the efficiency of the circulation control system. For blowing at supersonic jet speeds, shock boundary layer interactions on the Coanda surface can cause a detachment of the jet. As a result the circulation and lift are greatly reduced.

Experimental studies by Englar[4] and Alexander *et al.*[5] have shown that at higher speeds, the larger radius of curvature at the slot exit of elliptical Coanda surfaces offers an improvement in lift over smaller curvatures such as a circular Coanda shape (Fig. 2). Schlecht and Anders[6] also found that an elliptical Coanda surface was superior to a biconvex surface for both low subsonic and transonic freestreams.

Optimisation of circulation control aerofoils has focussed primarily on improving the efficiency of circulation control for STOL purposes.[7] As such the design conditions were limited to the subsonic flow regime. Many optimisation studies have investigated the effect of blowing rate, jet direction and location of a slot along an aerofoil[7–9] at low speeds. Studies investigating optimisation of the shape of the Coanda surface[10,11] have been performed, however in these studies both freestream and jet speeds were also designed for sub critical conditions.

Tai *et al.*[11] investigated the shape of the Coanda surface at the trailing edge of an elliptical aerofoil at a design condition of $M = 0.54$, $\alpha = -2.0°$ and $C_\mu = 0.0071$, using the TRACCON coupled inviscid-viscous solver.[12] It was found that an improvement in the lift coefficient of 27% was achieved at design conditions. Experiments were also conducted to investigate off-design behaviour of the optimised Coanda shape, which found no discernible improvement for $M = 0.73$ over a range of blowing coefficients.

Gradient based optimisation is an efficient and widely used method for aerodynamic shape optimisation problems, since it minimises the required number of flow solutions compared with other methods such as genetic algorithms. Gradient methods however require the derivatives of an objective function with respect to the design variables, which can be extremely expensive to compute when high fidelity CFD is employed. Gradient methods march along a direction, performing a one-dimensional minimisation before recomputing a new direction. Formally, the local minimum of the function is found when the gradient is zero.

Using the solution of the adjoint equations to provide gradients is a popular approach, as it reduces computational expense when compared with finite differencing for multiple design variables.[13,14] The cost of solving the adjoint equations is nearly independent of the number of design variables,[15] and scales only based on the number of cost functions of interest (such as C_d/C_l).

Using an optimisation scheme, the shape of an initial Coanda shape will be optimised to increase the lift coefficient generated due to a constant rate of blowing. The optimisation will be conducted for a design condition in cruise, with off design studies to follow. In addition to the cost benefit, the solution of the adjoint equation gives valuable information on the sensitivity of objective functions relative to local changes in geometry, as shown by Park and Green,[16] who investigated the placement of shape change effectors for control of a tailless delta wing configuration.

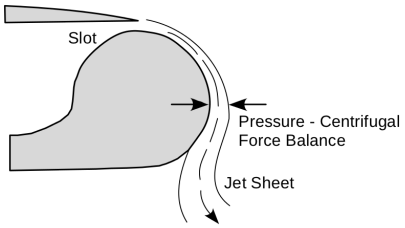

Figure 1: Trailing edge Coanda diagram.[5]

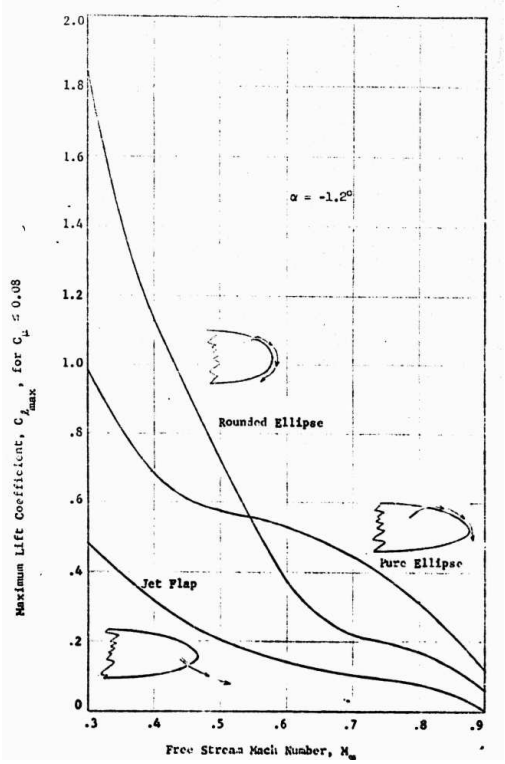

Figure 2: Maximum lift obtained by Englar with different Coanda geometries at range of Mach numbers for $C_\mu \leq 0.08$ on an elliptical aerofoil section.[4]

2. Methodology

2.1 HMB Navier–Stokes solver

The Helicopter Multi-Block (HMB) CFD code[17,18] was employed for this work. HMB solves the compressible, unsteady Reynolds-averaged Navier–Stokes equations on block-structured grids using a cell-centred finite-volume method for spatial discretisation. An implicit time-integration method is employed, and the resulting linear systems of equations are solved using a pre-conditioned Generalised Conjugate Gradient method. For unsteady simulations, an implicit dual-time stepping method is used, which is based on Jameson's pseudo-time integration approach.

The solver has a library of turbulence closures which includes several one and two-equation turbulence models and also non-Boussinesq versions of the $k-\omega$ model . Turbulence simulation is also possible using either Large-Eddy or Detached-Eddy simulation. Here, however, the baseline $k-\omega$ turbulence model of Wilcox[19] is used and a steady state solution is computed.

2.1.1 Reservoir boundary condition

Rather than imposing a jet exit profile, the flow is calculated from the plenum chamber within the aerofoil. The reservoir boundary condition fixes the pressure and density from the isentropic flow equations for a given nozzle pressure ratio, while the components of velocity are extrapolated assuming no gradients across the boundary. The quantities of turbulence on the reservoir boundary are extrapolated from the interior domain, which is initialised to freestream values.

2.2 Momentum coefficient

The supply of air into the plenum for circulation control is often taken from bleed air from the jet engine of the aircraft.[2] The jet momentum coefficient (C_μ) is a non-dimensional measure of blowing over a circulation control device, which is defined as

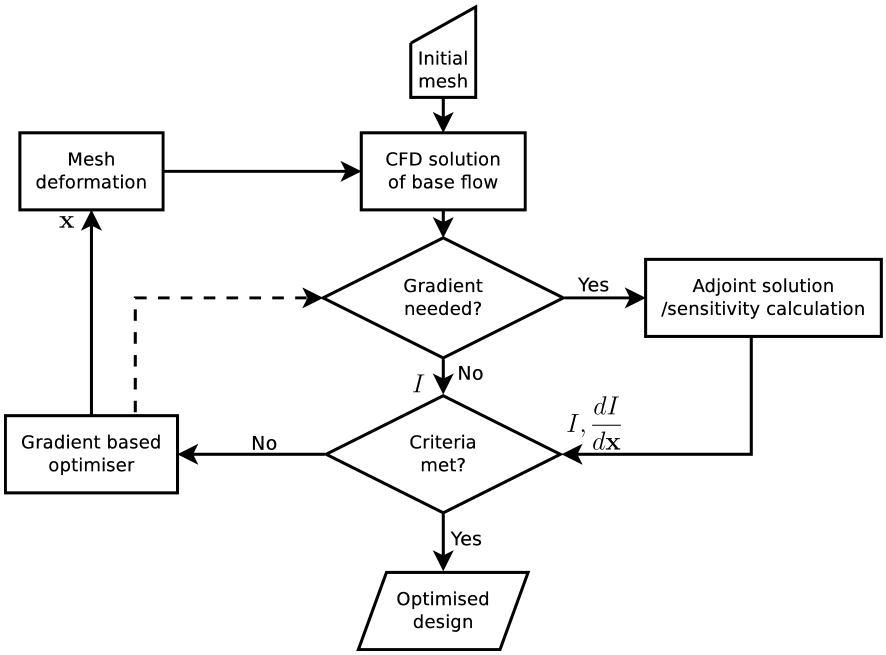

Figure 3: Flow chart of the optimisation process.

$$C_\mu = \frac{\dot{m}_j V_j}{q_\infty A} \tag{1}$$

where $\dot{m}_j$ is the mass flow rate through the slot exit, V_j the jet velocity, q_∞ the freestream dynamic pressure and A is the surface area of the aerofoil. In circulation control experiments, $\dot{m}_j$ is usually measured using a Venturi meter and V_j calculated from isentropic equations using the plenum pressure. In HMB, the plenum pressure ratio is fixed and the momentum coefficient is calculated a posteriori by integrating the solution along the slot exit.

2.3 Optimisation Routine

The HMB flow solver embeds a fully implicit adjoint solver,[20] which can be interfaced to any gradient based optimisation tool to solve design problems. The current implementation employs a Sequential Least Squares Quadratic Programming (SLSQP) optimisation algorithm[21,22] using the NLopt optimisation library.[23] The SLSQP uses the Broyden-Fletcher-Goldfarb-Shanno (BFGS) algorithm to update the approximation of the Hessian matrix.

Figure 3 summarises the design optimisation procedure. After the first calculation of the base flow and adjoint solutions for the initial design, the optimisation algorithm provides a new set of design variables ($\mathbf{x}$). The design variables then define the surface and volume mesh deformation which is passed into the CFD solver. To reduce computational expenditure, the adjoint sensitivity equations (for $dI/d\mathbf{x}$) are only computed when necessary. During the one-dimensional minimisation within the BFGS procedure, the gradients are not required and therefore the adjoint solution is not calculated, reducing the expense of the optimisation step by approximately 50%. The optimisation process is considered complete when either the gradient or the change in design variables between steps falls below a relative tolerance, typically 1×10^{-3}.

For the present study, the optimisation is conducted for a fixed angle of attack, freestream Mach number and nozzle pressure ratio. To enforce a constant blowing rate C_μ, the slot exit height and plenum shape are also fixed. A maximisation of the lift coefficient at these conditions will be performed, as such a minimisation of the objective function $I = -C_l$ is performed.

2.3.1 Adjoint sensitivity calculation

The gradient of the cost function ($dI/d\mathbf{x}$) is obtained by solving the sensitivity equation in adjoint form.[24,25] The underlying idea is to write explicitly the cost function I in terms of the flow variables $\boldsymbol{W}$ and design variables $\boldsymbol{x}$, i.e.

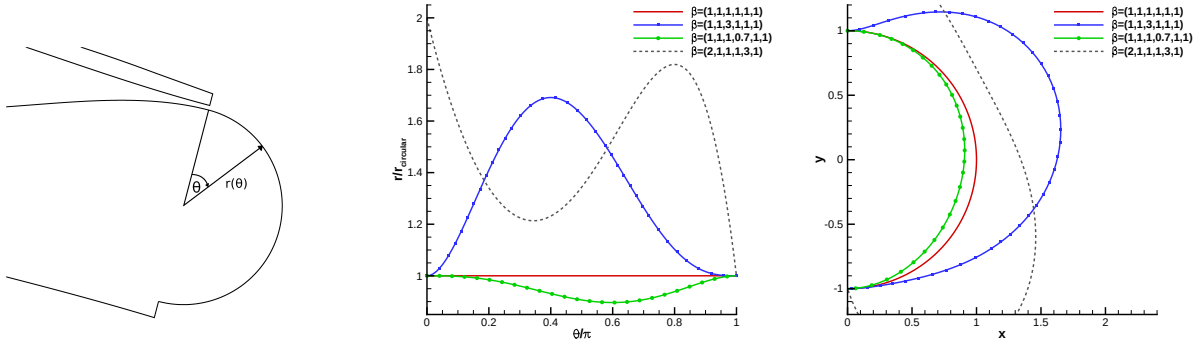

(a) Definition of parameters r and θ.

(b) Radial functions of sample Bernstein polynomials.

(c) Effective Coanda shape due to functions in Fig. 4b.

Figure 4: Parametrisation of Coanda surface by a radial distribution of Bernstein polynomials.

$I = I(\boldsymbol{W}(\boldsymbol{x}), \boldsymbol{x})$. The flow variables are subject to satisfy the Navier–Stokes equations, written in compact form as

$$\boldsymbol{R}(\boldsymbol{W}(\boldsymbol{x}), \boldsymbol{x}) = 0. \tag{2}$$

Formally, taking the derivative of I with respect to $\boldsymbol{x}$ we obtain:

$$\frac{\mathcal{D}I}{\mathcal{D}\boldsymbol{x}} = \frac{\partial I}{\partial \boldsymbol{x}} + \frac{\partial I}{\partial \boldsymbol{W}} \frac{\partial \boldsymbol{W}}{\partial \boldsymbol{x}}, \tag{3}$$

which represents the tangent form of the sensitivity equation. All the partial derivatives appearing on the right-hand side can be computed with limited effort, with the exception of $\partial \boldsymbol{W}/\partial \boldsymbol{x}$, which represents the variation of the flow variables with respect to the independent input parameters. This last term may be obtained by differentiating the governing equations (Eq. (2)), to yield the following linear system for the unknown $\partial \boldsymbol{W}/\partial \boldsymbol{x}$:

$$\frac{\partial \boldsymbol{R}}{\partial \boldsymbol{W}} \frac{\partial \boldsymbol{W}}{\partial \boldsymbol{x}} = -\frac{\partial \boldsymbol{R}}{\partial \boldsymbol{x}}. \tag{4}$$

The solution of Eq. (4) must be solved for each design variable to compute the sensitivities, since the right-hand side of Eq. (4) depends upon $\boldsymbol{x}$. Therefore, the computational cost scales with the number of design variables. The sensitivity problem (Eqs. (3) and (4)) can be recast in dual form by introducing the adjoint vector variable $\boldsymbol{\lambda}$ as the solution of the following linear system:

$$\left(\frac{\partial \boldsymbol{R}}{\partial \boldsymbol{W}}\right)^{\mathrm{T}} \boldsymbol{\lambda} = -\left(\frac{\partial I}{\partial \boldsymbol{W}}\right)^{\mathrm{T}}. \tag{5}$$

Substituting equation Eq. (5) into Eq. (3) and using matrix algebra we obtain:

$$\frac{\mathcal{D}I}{\mathcal{D}\boldsymbol{x}} = \frac{\partial I}{\partial \boldsymbol{x}} + \boldsymbol{\lambda}^{\mathrm{T}} \frac{\partial \boldsymbol{R}}{\partial \boldsymbol{x}}. \tag{6}$$

The computational cost of the dual sensitivity problem (Eqs. (5) and (6)) scales with the number of outputs, since the right-hand side of Eq. (5) depends on I, but it is independent of the input parameters. The adjoint form of the sensitivity equation is therefore particularly efficient for aerodynamic optimisation applications, where usually the number of cost functional is small while the number of design variables is large.

2.3.2 Coanda parametrisation

In the current work the Coanda surface is parametrised by a radial function varying with the angle, θ from the jet exit (see Fig. 4a). The function chosen is based on the summation of Bernstein polynomials, given by;

$$r(\theta) = B_n\left(\frac{\theta}{\pi}\right) = \sum_{\nu=0}^{n} \beta_\nu b_{\nu,n}\left(\frac{\theta}{\pi}\right), \tag{7}$$

where

$$b_{\nu,n}(t) = \binom{n}{\nu} t^\nu (1-t)^{n-\nu}, \quad t \in [0,1]. \tag{8}$$

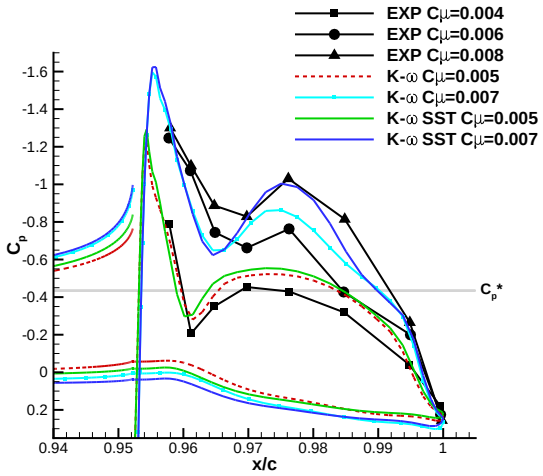

(a) Distribution over the Coanda surface with blowing.

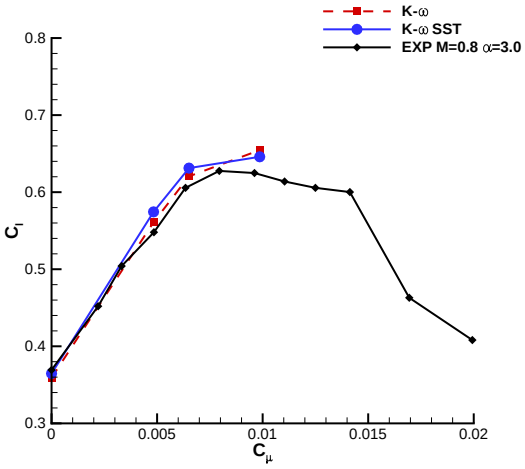

(b) Comparing sectional lift coefficient due to blowing of simulated and experimental circulation control data.

Figure 5: Validation against NASA experiment[5] with a freestream of $M = 0.8$ and $\alpha = 3.0°$.[27]

The vector of coefficients β_ν is fixed such that $\beta_0 = \beta_1 = \beta_{n-1} = \beta_n = 1.0$. Limiting the coefficients at the slot exit(s) in this way forces the surface contours to be continuously differentiable at the exit. Figures 4b and 4c demonstrate this necessity, with β_0 or $\beta_n \neq 1.0$ the Coanda surface does not meet the slot exit, while β_1 or $\beta_{n-1} \neq 1.0$ creates a discontinuity in curvature. A resulting Coanda surface defined by n design variables (given by the vector $\boldsymbol{x}$) will require $n + 4$ β-coefficients.

2.3.3 Grid deformation

The deformation of the volume grid is achieved by an Inverse Distance Weighting (IDW) method.[26] IDW is an interpolation method that calculates the values at a given point using a weighted average of the values from a set of known sample points. The weight assigned to the value at a known point is proportional to the inverse of the distance between itself and the point to be deformed.

The position of points belonging to parametrically deformed surfaces (Section 2.3.2) are provided to the CFD solver. Displacement within the remainder of the domain are interpolated by the IDW method from these sample surface points, such that the grid deformation does not deteriorate the grid quality and does not lead to invalid cells (*e.g.* negative volumes).

3. Preliminary Study of Circulation Control

3.1 Validation Against NASA Transonic Circulation Control Experiment

A previous study[27] of transonic circulation control was conducted against the experiments performed by Alexander *et. al.*[5] Three-dimensional RANS simulations were necessary to represent the flow over the elliptical section, finite span wing. Significant angle of attack corrections were required for two-dimensional simulations to agree with the pressure distribution on the upper and lower surfaces of the main aerofoil section, however the pressure distribution on the Coanda surface were predicted with reasonable accuracy in both two and three-dimensional simulations.

It was found that for moderate blowing rates the pressure distribution on the Coanda surface and the generated lift were in good agreement with the experiment, as shown in Figs. 5a and 5b. The difference between two variants of the $k - \omega$ turbulence model was minimal for low blowing rates.

3.2 Supercritical Aerofoil Test Case

The supercritical DLBA032 aerofoil section was chosen from the AGARD CFD validation database[28] due to the availability of experimental data with an aileron deflection in a transonic freestream. The McDonnell Douglas DLBA032 is a supercritical aerofoil with a thickness of 12% chord and an aileron of 25% chord length. Experiments were conducted

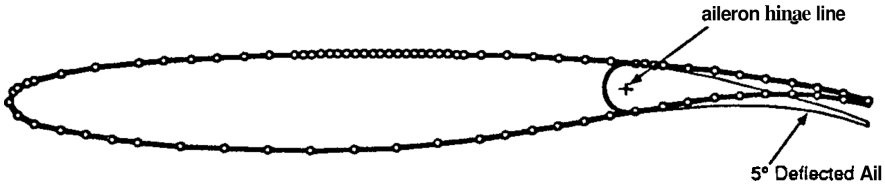

(a) Original geometry with aileron deflection.[28]

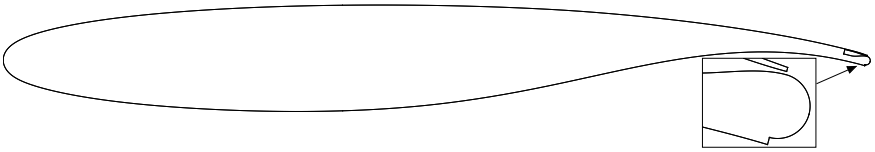

(b) Modified geometry with circulation control device.

Figure 6: Douglas DLBA032 geometry.

at a Reynolds number range of $Re = 5 \times 10^6$ to $Re = 25 \times 10^6$, an aileron deflection of $\alpha_{AIL} = -5°$ to $\alpha_{AIL} = 5°$ and $M \approx 0.72$. It was reported that the experiment was suitable for two-dimensional CFD studies.[28]

Figure 6 shows the modifications that were made to the geometry of the DLBA032 aerofoil. The trailing edge was thickened to allow for a Coanda device with a radius of 0.525% chord and a slot height of 0.025% chord. The geometry was designed to allow for blowing from both upper and lower slots, however here we focus upon upper surface blowing only (as shown in the inset of Fig. 6b).

In a previous work, two dimensional CFD studies[27] were conducted on this aerofoil configuration for $M = 0.715$ and $Re \approx 5 \times 10^6$. A summary of the results from these studies are presented in Sections 3.2.1 and 3.2 for completeness. A comparison of the behaviour of a circulation control device on the trailing edge with that of a deflected aileron was conducted. Although the shock position of the aileron-deflected cases was predicted too far downstream of the experimental findings, it was found that predictions of blowing over a Coanda device has the ability to match the predicted lift achieved by a 3° aileron in transonic conditions for an angle of attack range of $0° \leq \alpha \leq 4°$.[27] Table 1 summarises the simulated and experimental results for the DLBA032 with aileron deflections, and also the baseline circular Coanda shape with blowing at a pressure ratio of $NPR = 4.0$.

Table 1: Comparing sectional lift, drag, and pitching moment behaviour of the DLBA032 at $M \approx 0.715$ and $Re \approx 5 \times 10^6$ with and without aileron deflection.

Angle of Attack (°)	Aileron Angle (°)/ Nozzle Pressure Ratio	Data Source	C_l	C_d	C_m
$\alpha = 1.342$	$\alpha_{AIL} = 0.0$	Experiment[28]	0.7311	0.0104	-0.1518
$\alpha = 1.342$	$\alpha_{AIL} = 0.0$	CFD	0.7823	0.0167	-0.1614
$\alpha = 1.183$	$\alpha_{AIL} = 3.0$	Experiment[28]	0.8931	0.0142	-0.1787
$\alpha = 1.183$	$\alpha_{AIL} = 3.0$	CFD	1.0460	0.0236	-0.2073
$\alpha = 1.342$	$\alpha_{AIL} = 3.0$	CFD	1.0827	0.0255	-0.2098
$\alpha = 1.342$	Unblown Coanda	CFD	0.8251	0.0183	-0.1710
$\alpha = 1.342$	$NPR = 4.0$ Coanda	CFD	1.1527	0.0268[a]	-0.2458

[a] C_d here for circulation control excludes the effect of jet momentum.

3.2.1 Baseline circulation control simulation

All cases presented here were simulated with a freestream Mach number of $M = 0.716$, angle of attack $\alpha = 1.342°$ and Reynolds number $Re = 5.028 \times 10^6$ using the Wilcox $k - \omega$ turbulence model. A grid independence study found minimal difference between the integrated loads of two-dimensional meshes with 5×10^5 and 2.5×10^5 cell volumes, both having $y^+ = 1.0$. To reduce computational expense, the 2.5×10^5 cell volume mesh was used throughout the optimisation process.

Figure 7 shows Mach contours at the trailing edge of the aerofoil with blowing from a nozzle at a pressure ratio of $NPR = 4.0$ over a circular Coanda with a radius:slot height ratio of 21:1. The jet remains attached to the Coanda surface until an angle of approximately 100° from the slot exit. As a result of this attachment, the lift coefficient from

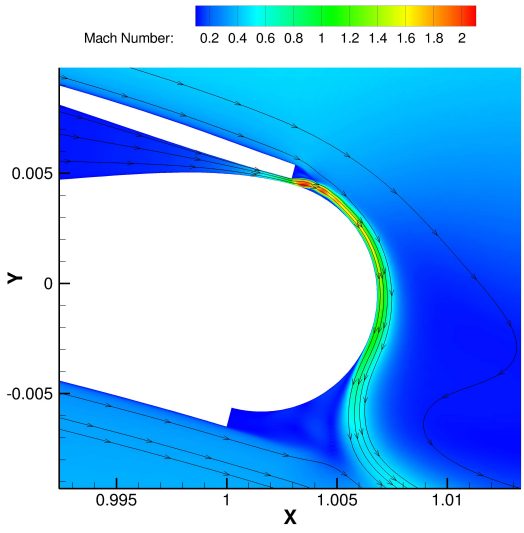

Figure 7: Contours of Mach number for the trailing edge of the circular Coanda baseline case at nozzle pressure ratio $NPR = 4.0$, $C_l = 1.1527$.

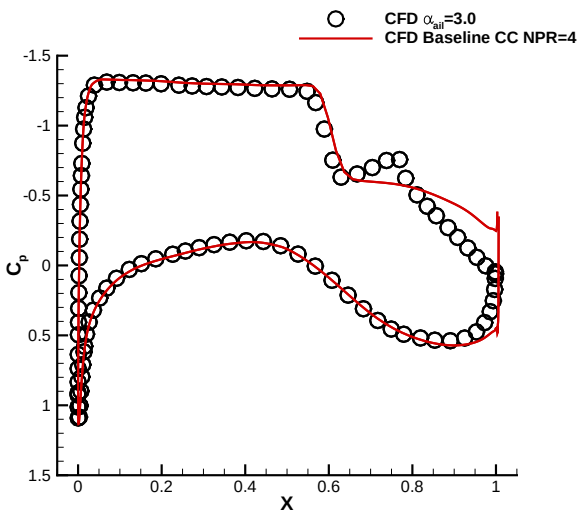

Figure 8: Comparison between pressure coefficients of baseline case and a 3° deflected aileron, $M = 0.716$, $\alpha = 1.342°$, $Re = 5.028 \times 10^6$.

the additional circulation is approximately 6.5% higher than that of a 3° deflected aileron. The pressure coefficients for the baseline CC geometry and simulated aileron deflection are shown in Fig. 8, the suction peak at the trailing edge contributed to a 17% increase in the pitching moment coefficient for CC compared with that of the aileron.

Comparing the relative changes due to the deflection of the aileron and blowing over the circular Coanda gives $\Delta C_l = 0.3$ and $\Delta C_{lBaseline} = 0.33$, respectively. This baseline $\Delta C_{lBaseline}$ will be taken as the reference with which the performance of the all designs within the optimisation procedure will be compared.

4. Optimisation Results

4.1 Circular Initialisation

The optimiser was initialised with 5 design variables set to the baseline geometry shown in Section 3.2.1, corresponding to the vector $\boldsymbol{x}_{baseline} = [1.0, 1.0, 1.0, 1.0, 1.0]$ which describes the line $r = r_{baseline} = 5.25 \times 10^{-3} c$. The design variables were limited to $\boldsymbol{x}_{min} = [0.7, 0.7, 0.7, 0.7, 0.7]$ and $\boldsymbol{x}_{max} = [1.10, 1.30, 2.50, 1.30, 1.10]$, which is shown in Fig. 9. Between the limits, a wide range of smooth Coanda surfaces can be generated, represented by the summation of 9 Bernstein polynomials, as described in Section 2.3.2.

The surface sensitivities of the baseline circular shape are shown in Fig. 10. The sensitivities of the lift coefficient are greatest at the locations of separation and the oblique shock due to the under expansion. The oblique shocks and separation bubble due to the underexpansion gave large values of dC_l/dX_n, indicating that the effects of the underexpansion of the jet near the slot exit significantly influences the effectiveness of the circulation control device. In the location of the shock induced separation, the direction of the surface deformation is inclined towards an outward displacement, while where the jet detached from the Coanda surface an inwards deformation gives an increase in C_l. As a result, the gradient from the baseline circular shape is:

$$\frac{dC_l}{d\boldsymbol{x}} = \begin{bmatrix} 1.13011 \times 10^{-1} \\ 3.22887 \times 10^{-2} \\ -3.07652 \times 10^{-2} \\ -4.02053 \times 10^{-2} \\ 1.63244 \times 10^{-2} \end{bmatrix}^{\mathrm{T}} \tag{9}$$

As the optimiser performed a line search in a direction influenced by Eq. (9), a shape was found that caused the jet to detach, see Fig. 11. The high rate of curvature near the slot exit formed a pressure gradient that was too high for the supersonic jet to overcome. Along the line search, the maximum of the first design variable was set by the optimiser, while the other variables were relatively unchanged. This detachment of the jet significantly reduced the objective function, which is visible in the second iteration of Fig. 12.

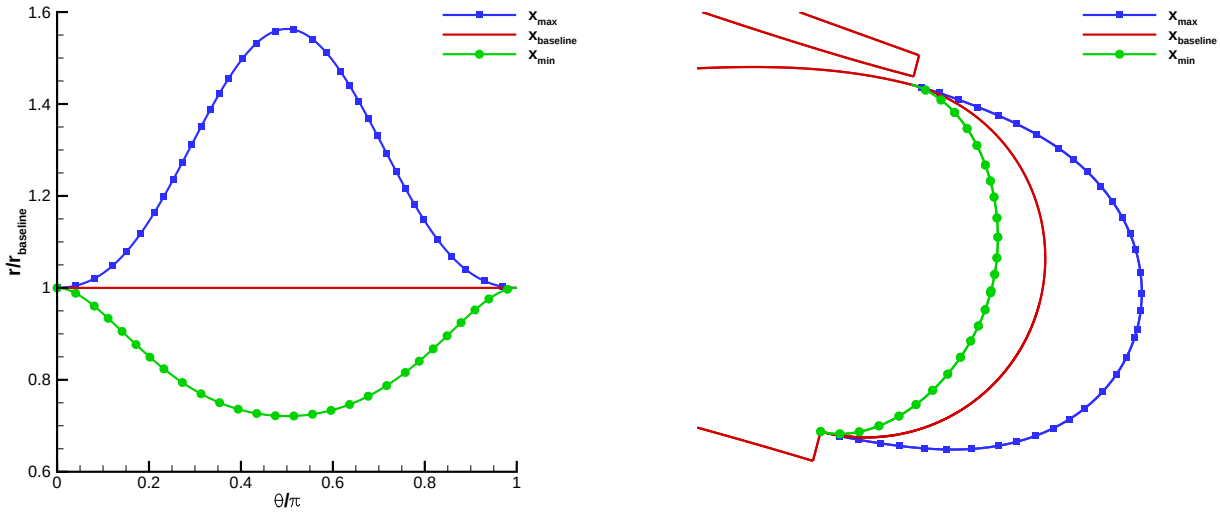

(a) Bernstein polynomial representation.

(b) Physical representation of parameters on Coanda surface.

Figure 9: Schematic of the baseline and design variable limit parameters.

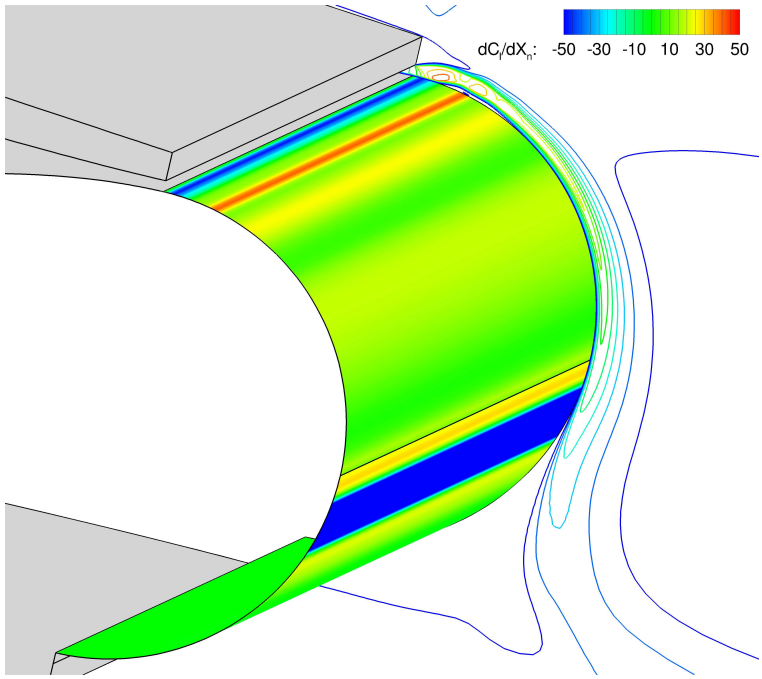

Figure 10: Surface sensitivities (solid colours) of the circular Coanda, showing the sensitivity of the lift coefficient with respect to a cell displacement normal to the surface. Red colours indicate a local tendency towards an outward displacement. For illustration, contours of Mach number are plotted as lines, as also shown in Fig. 7.

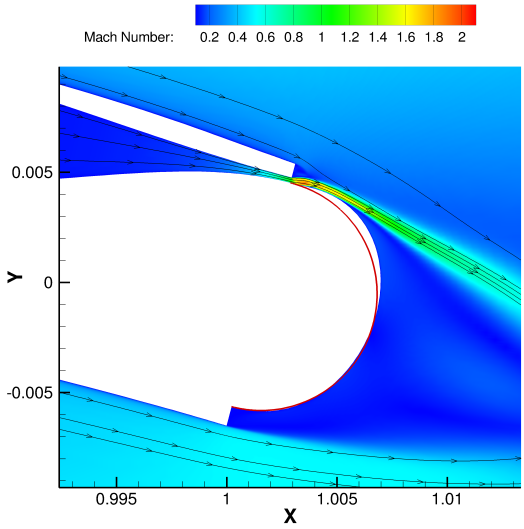

Figure 11: Contours of Mach number at the trailing edge for the second iteration of the CFD solution. Red lines show the original geometry. $C_l = 0.9503$.

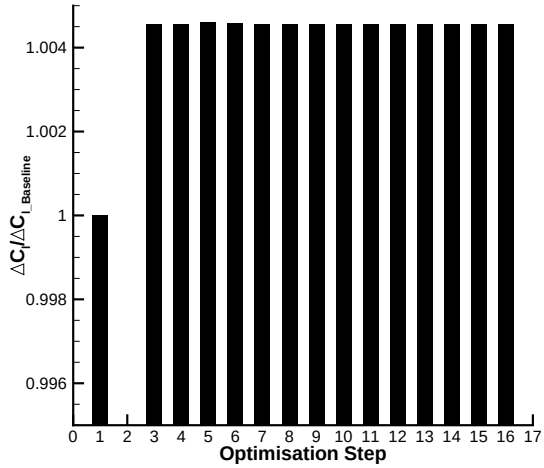

Figure 12: Bar chart showing the relative change in lift coefficient increase with respect to every function call of the CFD solver. The change is relative to the original baseline $\Delta C_l = 0.33$, a 0.45% increase in efficiency of the CC system is found.

The following iteration of the optimisation procedure converged to a solution where the jet remained attached to the Coanda. This third iteration concluded the line search as an estimate of the minimum was found. A new direction and line search was conducted from the fourth iteration onwards. In this direction however, a minimum was not found and by the 16$^{\text{th}}$ function iteration, the optimiser converged to a stable solution. A small overall increase in the lift coefficient was observed, $C_l - C_{lBaseline} = 0.0015$, which corresponded to design variables given by Eq. (10):

$$\boldsymbol{x} = \begin{bmatrix} 1.00999 \\ 1.00325 \\ 0.99692 \\ 0.99596 \\ 1.00164 \end{bmatrix}^{\mathrm{T}} \tag{10}$$

These values resulted in a near-negligible difference in the Coanda shape from the original baseline shape. It is possible that the original circular shape was close to a local optimum in the design space.

4.2 Quasi-elliptical Initialisation

Starting with a 5 parameter design of $\boldsymbol{x}_{initial} = [1.0, 1.0, 2.0, 1.0, 1.0]$, which gives a shape similar to that of a 1.25 aspect ratio ellipse, resulted in an initial lift coeefficient of $C_l = 1.1129$, 3.5% lower than the original circular baseline geometry generated. Although this initial case failed to improve upon the generated lift than the baseline case (see Fig. 13), after 6 optimisation steps the optimiser had found a Coanda shape with a higher lift coefficient than the previous circular optimisation result.

Again a state for which the jet detached was found, at the 7$^{\text{th}}$ iteration. Figure 14 shows some of the changes in which the optimiser directed the Coanda shape. Green circles indicate the surface of the 7$^{\text{th}}$ optimiser iteration. The high rate of curvature at approximately 45° caused detachment of the jet as with the previous circular case.

Figure 15 shows the effect of the optimisation on the detachment location of the Coanda jet. For the 18$^{\text{th}}$ step (Fig. 15b) the jet remained attached much longer to the Coanda, increasing the circulation and effective camber of the aerofoil. While not shown here, the shock position due to this effective change in camber was moved towards the trailing edge by approximately 10% chord.

A comparison of the surface sensitivities between the initial quasi-elliptical and optimised (18$^{\text{th}}$ step) Coanda surfaces is shown in Fig. 16. Although there are some regions of relatively high sensitivity near the jet exit and at the region of detachment, the optimised solution significantly reduced the magnitude of the sensitivities for the region in which the jet remains attached to the Coanda.

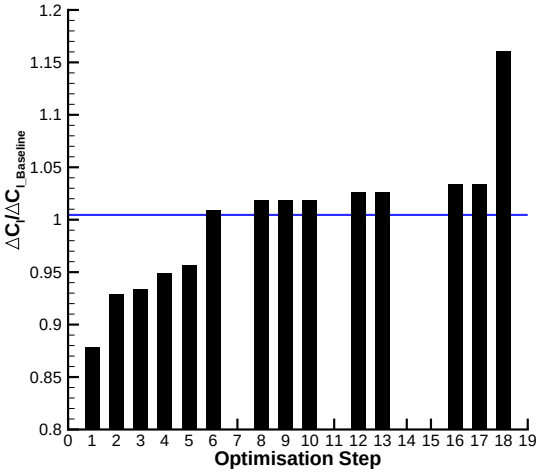

Figure 13: Bar chart showing the relative change in lift coefficient increase with respect to every function call of the CFD solver. The change is relative to the original circular baseline $\Delta C_l = 0.33$. The horizontal line indicates the maximum achieved from the circular optimisation (Fig. 12).

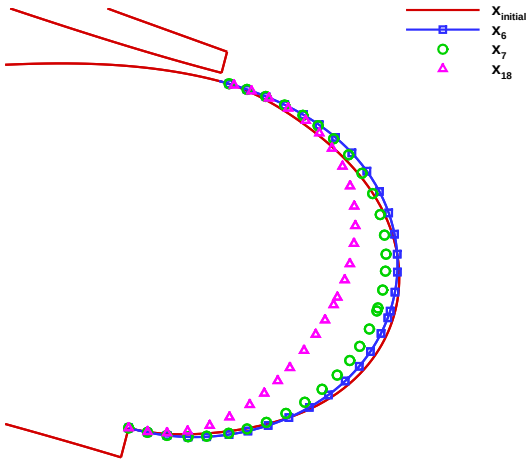

Figure 14: Coanda contours from the near elliptical starting configuration.

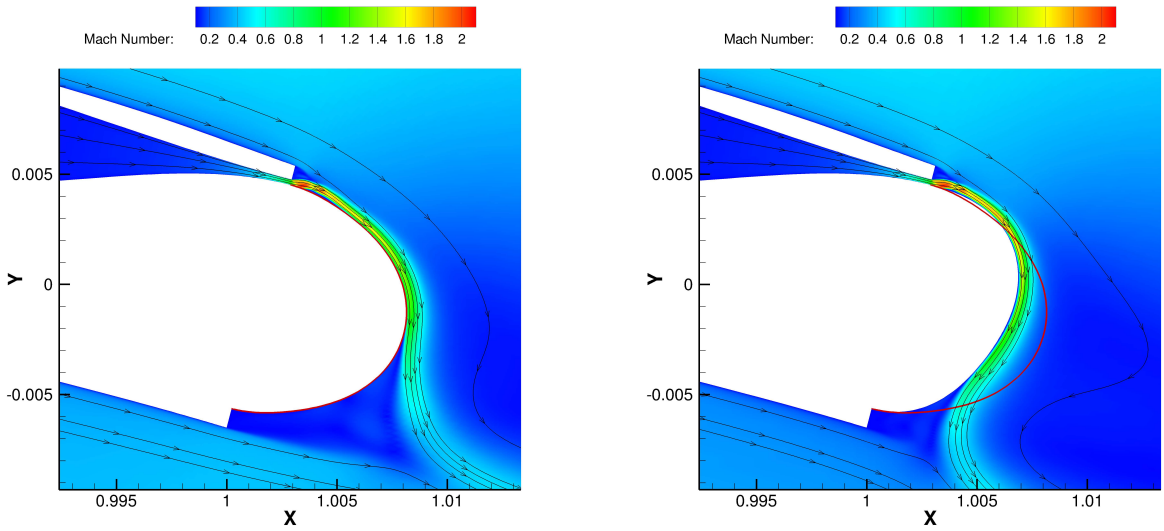

(a) Initial quasi-elliptical Coanda shape, $C_l = 1.1129$.

(b) After 18th optimisation step, $C_l = 1.2052$.

Figure 15: Contours of mach number at the trailing edge of the aerofoil.

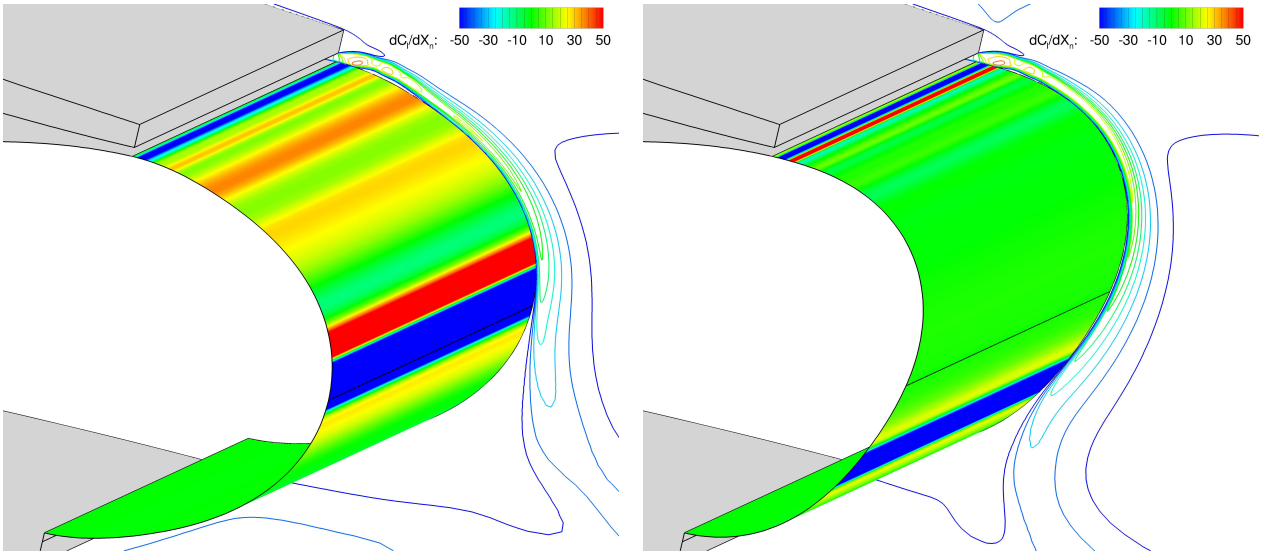

(a) Initial quasi-elliptical Coanda shape, C_l = 1.1129.

(b) After 18th optimisation step, C_l = 1.2052.

Figure 16: Contours of surface sensitivity of the Coanda surface.

5. Conclusions and Future Work

Using a gradient based optimisation scheme, it has been shown that the design of Coanda surfaces can be optimised with a relatively small computational cost. An increase in up to 8% of the C_l was found when starting from a simple quasi-elliptical shape. With this optimised design, the ΔC_l increased by approximately 16% compared with the baseline circular case at no additional cost due to blowing, i.e. with the same momentum coefficient C_μ.

The contours of sensitivity as discussed in Section 4.1 suggest that controlling the under-expansion of the jet will help improve the efficiency of the Coanda device. Further investigations into the optimisation of the Coanda shape with a step using an under-expanded jet will be conducted, and without the step but with a correctly expanded jet will follow.

Even if limitations were imposed on the design variables, at certain cycles of the optimisation, geometries were produced which caused detachment of the jet. This detachment phenomenon created a series of steep peaks and troughs in the design space which could hinder the convergence of gradient based methods. Despite these concerns over the smoothness of the design space, the SLSQP algorithm converged to an optimal solution, characterised by a significant increase in the lift gain due to blowing.

Off design behaviour of the optimised transonic circulation control device is in progress, which includes a range of blowing rates, angles of attack and Mach numbers. A study to improve the behaviour of an initially detached Coanda jet will also follow.

Acknowledgements

The present research was supported by a doctoral scholarship from the Engineering and Physical Sciences Research Council of the UK, with additional sponsorship from BAE Systems and DSTL through the industrial CASE Award scheme. Dr. M. Biava is supported by the LOCATE project of Hybrid Air Vehicles and Innovate UK.

References

[1] Englar, R. J. and Huson, G. G., "Development of Advanced Circulation Control Wing High-Lift Airfoils." *Journal of Aircraft*, Vol. 21, No. 7, 1984, pp. 476–483.

[2] Cook, M. V., Buonanno, A., and Erbslöh, S. D., "A Circulation Control Actuator for Flapless Flight Control," *Aeronautical Journal*, Vol. 112, No. 1134, 2008, pp. 483–489.

[3] Abramson, J. and Rogers, E. O., "High Speed Characteristics of Circulation Control Airfoils," *AIAA 21st Aerospace Sciences Meeting*, AIAA, 10/01 1983.

[4] Englar, R. J., "Two-Dimensional Transonic Wind Tunnel Tests of Three 15-Percent Thick Circulation Control Airfoils," Tech. Rep. AD882075, DTNSRDC, 1970.

[5] Alexander, M. G., Anders, S. G., Johnson, S. K., Florance, J. P., and Keller, D. F., "Trailing Edge Blowing on a Two-Dimensional Six-Percent Thick Elliptical Circulation Control Airfoil up to Transonic Conditions," Tech. Rep. TM-2005-213545, NASA, 2005.

[6] Schlecht, R. and Anders, S. G., "Parametric Evaluation of Thin, Transonic Circulation-Control Airfoils," *45th AIAA Aerospace Sciences Meeting*, Vol. 5, 8th-11th January 2007, pp. 3374–3398.

[7] Loth, J. L. and Boasson, M., "Circulation Controlled STOL Wing Optimization," *Journal of Aircraft*, Vol. 21, No. 2, 1984, pp. 128–134.

[8] Meunier, M., "Simulation and Optimization of Flow Control Strategies for Novel High-Lift Configurations," *AIAA Journal*, Vol. 47, No. 5, Jan-1 2009, pp. 1145–1157.

[9] Djojodihardjo, H., Majid, A. A., Laila, D., Romli, F. I., Basri, S., Hamid, A., and Faisal, M., "Numerical Simulation and Analysis of Coanda Effect Circulation Control for Wind-Turbine Application Considerations," *IIUM Engineering Journal*, Vol. 12, No. 3, 2011, pp. 19–42.

[10] Tai, T. C., Kidwell, G. H., and Vanderplaats, G. N., "Numerical Optimization of Circulation Control Airfoils." *Journal of Aircraft*, Vol. 19, No. 2, 1982, pp. 145–150.

[11] Tai, T. C. and Kidwell, G. H., "Numerical Optimization of Circulation Control Airfoil at High Subsonic Speed." *Journal of Aircraft*, Vol. 22, No. 10, 1985, pp. 869–874.

[12] Dvorak, F. A. and Choi, D. H., "Analysis of Circulation-Controlled Airfoils in Transonic Flow," *Journal of Aircraft*, Vol. 20, No. 4, 1983, pp. 331–337.

[13] Jameson, A., Martinelli, L., and Pierce, N. A., "Optimum aerodynamic design using the Navier-Stokes equations," *Theoretical and Computational Fluid Dynamics*, Vol. 10, No. 1-4, 1998, pp. 213–237.

[14] Kim, H. J., Sasaki, D., Obayashi, S., and Nakahashi, K., "Aerodynamic optimization of supersonic transport wing using unstructured adjoint method," *AIAA Journal*, Vol. 39, No. 6, 2001, pp. 1011–1020.

[15] Nemec, M., Zingg, D. W., and Pulliam, T. H., "Multipoint and multi-objective aerodynamic shape optimization," *AIAA Journal*, Vol. 42, No. 6, 2004, pp. 1057–1065.

[16] Park, M. A., Green, L. L., Montgomery, R. C., and Raney, D. L., "Determination of Stability and Control Derivatives using Computational Fluid Dynamics and Automatic Differentiation," *Proceedings of the 17th AIAA Applied Aerodynamics Conference; June 28-July 1 1999, Norfolk VA; AIAA Paper*, 1999, p. 3136.

[17] Steijl, R., Barakos, G., and Badcock, K., "A Framework for CFD Analysis of Helicopter Rotors in Hover and Forward Flight," *Int. J. Numer. Meth. Fluids*, Vol. 51, 2006, pp. 819–847.

[18] Barakos, G., Steijl, R., Badcock, K., and Brocklehurst, A., "Development of CFD Capability for Full Helicopter Engineering Analysis." 31st European Rotorcraft Forum, 13-15 September 2005, Florence, Italy, 2005.

[19] Wilcox, D. C., "Formulation of the k-ω Turbulence Model Revisited," *AIAA Journal*, Vol. 46, No. 11, 2008, pp. 2823–2838.

[20] Biava, M., Woodgate, M., and Barakos, G. N., "Discrete Adjoint Methods for the Computation of Rotorcraft Aerodynamic Derivatives," *53rd AIAA Aerospace Sciences Meeting*, American Institute of Aeronautics and Astronautics, 5th-9th Jan 2015.

[21] Kraft, D. et al., "A Software Package for Sequential Quadratic Programming," Tech. Rep. DFVLR-FB 88-28, Institut für Dynamik der Flugsysteme, Oberpfaffenhofen, Germany, 1988.

[22] Kraft, D., "Algorithm 733: TOMP–Fortran Modules for Optimal Control Calculations," *ACM Transactions on Mathematical Software (TOMS)*, Vol. 20, No. 3, 1994, pp. 262–281.

[23] Johnson, S. G., "The NLopt Nonlinear-optimization Package," http://ab-initio.mit.edu/nlopt, 2014.

[24] Limache, A. C. and Cliff, E. M., "Aerodynamic Sensitivity Theory for Rotary Stability Derivatives," *Journal of Aircraft*, Vol. 37, No. 4, 2000, pp. 676–683.

[25] Mader, C. A. and Martins, J. R. R. A., "Computation of Aircraft Stability Derivatives using an Automatic Differentiation Adjoint Approach," *AIAA Journal*, Vol. 49, No. 12, 2011, pp. 2737–2750.

[26] Shepard, D., "A Two-dimensional Interpolation Function for Irregularly-spaced Data," *Proceedings of the 1968 23rd ACM National Conference*, ACM '68, ACM, New York, NY, USA, 1968, pp. 517–524.

[27] Forster, M. and Steijl, R., "Numerical Simulation of Transonic Circulation Control," *53rd AIAA Aerospace Sciences Meeting*, American Institute of Aeronautics and Astronautics, 5th-9th Jan 2015.

[28] Elsenaar, A., Waggoner, E. G., and Ashill, P. R., "A Selection of Experimental Test Cases for the Validation of CFD Codes," Tech. Rep. AR-303, AGARD, 1994.